Colloids and Surfaces A 570 (2019) 165–171

Contents lists available at ScienceDirect

Colloids and Surfaces A

journal homepage: www.elsevier.com/locate/colsurfa

Facile aqueous, room temperature preparation of high transverse relaxivity clustered iron oxide nanoparticles

Nicholas J. Hobson[a,b], Xian Weng[a,b], Marianne Ashford[c], Nguyen T.K. Thanh[b,d], Andreas G. Schätzlein[a], Ijeoma F. Uchegbu[a,*]

[a] UCL School of Pharmacy, 29-39 Brunswick Square, London, WC1N 1AX, UK
[b] UCL Healthcare Biomagnetic and Nanomaterials Laboratories, 21 Albemarle Street, London, W1S 4BS, UK
[c] AstraZeneca, Charter Way, Macclesfield, UK
[d] Department of Physics & Astronomy, UCL, Gower Street, London, WC1E 6BT, UK

GRAPHICAL ABSTRACT

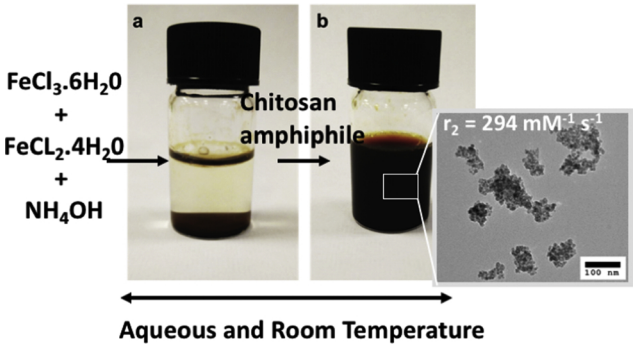

ARTICLE INFO

Keywords:
SPIONs
Iron oxide nanoparticles
Superparamagnetic
GCPQ
N-palmitoyl-*N*-monomethyl-*N*,*N*-dimethyl-*N*,*N*,*N*-trimethyl-6-*O*-glycolchitosan
Chitosan
T2-weighted
Colloid
Relaxivity

ABSTRACT

Clustering superparamagnetic iron oxide nanoparticles (SPIONs) is one method of providing the biomedical benefits of larger SPIONs [e.g. superior T2 weighted magnetic resonance imaging (MRI) contrast] without increasing particle size. The work presented herein, describes the facile synthesis of clustered SPIONs that are suitable for MRI applications, by using a chitosan based polymer: N-palmitoyl-*N*-monomethyl-*N*-N-dimethyl-*N*-N-*N*-trimethyl-6-O-glycolchitosan (GCPQ) and aqueous nanoprecipitation followed by probe sonication, in the absence of organic solvents or elevated temperatures. The resulting clustered SPIONs consist of individual 8 nm iron oxide nanoparticles clustered into a 150 nm particle with a positive zeta potential (+23 mV) at neutral pH. X-ray diffraction confirms the presence of crystalline magnetic iron oxide, while magnetometer experiments show the clustered SPIONs are superparamagnetic giving an overall M_s of 63.5 ± 1.3 emu g^{-1}. Relaxometry analyses revealed that the clustered SPIONs (inclusive of coatings) had a high r_2 value of 294.8 mM^{-1} s^{-1} and an r_2/r_1 of 21.1 making the clustered SPIONs suitable for T2 weighted (negative) MRI contrast imaging applications. The resulting clustered SPIONs demonstrate that highly sensitive T2 contrast agents may be produced in mild room temperature conditions, without the need for organic solvents or low molecular weight surfactants.

* Corresponding author at: UCL School of Pharmacy, 29-39 Brunswick Square, London, WC1N 1AX, UK.
E-mail address: ijeoma.uchegbu@ucl.ac.uk (I.F. Uchegbu).

https://doi.org/10.1016/j.colsurfa.2019.03.023
Received 15 November 2018; Received in revised form 9 March 2019; Accepted 10 March 2019
Available online 11 March 2019

1. Introduction

Superparamagnetic iron oxide nanoparticles (SPIONs) and other iron oxide nanoparticles are widely considered for biomedical applications due to their good biocompatibility and attractive therapeutic and diagnostic properties [1,2]. SPIONs have thus been used to generate therapeutic hyperthermia in the clinic [3], treat anaemia [4], accomplish magnetic targeting of therapeutics [5,6] or as magnetic resonance imaging (MRI) T2 weighted (negative) contrast reagents [7]. Despite their advantageous biomedical properties, a number of clinically approved iron oxide imaging agents have recently been withdrawn [8–11]. While the precise reasons for product withdrawal is never stated, clinical uptake was obviously a factor, due presumably to the poor MRI image contrast obtained with these agents, when compared to gadolinium based agents [12]. However gadolinium contrast agents are associated with brain and bone accumulation as well as kidney toxicity [13], justifying the search for more biocompatible, yet effective imaging agents.

Clustering SPIONs leads to improved T2 weighted imaging, due to the significant lowering of the T2 (transverse magnetisation or spin - spin) relaxation time; improving image resolution in the liver vasculature for example [14], making clustering a viable method of achieving efficient imaging with SPIONs. Clustering of sub 10 nm nanoparticles will ensure improvements in T2 weighted imaging while ensuring eventual excretion of the SPIONs [15]. Non-covalently clustered SPIONs are usually prepared by clustering hydrophobically coated iron oxide nanoparticles [16]. Hydrophobically coated iron oxide nanoparticles are prepared at high temperature (> 200 °C) and in organic solvents [17]. These nanoparticles with a hydrophobic coating (usually oleic acid) are then encapsulated within either polymeric [16] or low molecular weight [18] amphiphiles to produce the clusters; with the clustering achieved by mixing the non-aqueous phase containing the hydrophobically coated iron oxide nanoparticles with the amphiphile in the aqueous phase, followed by evaporation of the organic solvent layer. Hydrophobic polymers, such as poly(lactide-co-glycolide) [19] or hydrophilic polymers such as poly(ethylene glycol) [20] may also be used to encapsulate the hydrophobic iron oxide nanoparticles within a larger cluster. Others have reported the preparation of hydrophobized iron oxide particles using lower temperatures of 90 °C followed by separation of the colloidal fraction by centrifugation and then mixing of the colloidal fraction with phospholipid amphiphiles [21]. High temperatures (95–260 °C) are routinely used in the clustering techniques [17,22]. Another form of clustering uses colloidal iron oxide coated with ferritin by using high temperatures (60 °C) to make magnetoferritin [23] followed by clustering using a cationic amphiphilic polymer to bind to the anionic ferritin coating [24]. All the methods thus far reported [25–30] require both above ambient temperatures to at least 60 °C and/ or organic solvents, making them resource intensive and encumbering these formulations with the need to demonstrate the absence of residual organic solvents. Where lower temperatures are used and organic solvents excluded for clustering the resulting clustered SPIONs exhibit relatively low r_2 relaxivities (< 200 mM s^{-1} when measured at 1.5 T) [31–33]. We hypothesised that clustering would be achieved by simply mixing the nanoprecipitated iron oxide crystals, precipitated at ambient temperature, with an amphiphilic polymer, thus avoiding the need for organic solvents and above ambient temperatures. Here we report a facile method of clustering SPIONs involving the ambient alkaline nanoprecipitation of the SPIONs followed by clustering at room temperature by using use an amphiphilic chitosan: N-palmitoyl-*N*-monomethyl-*N*-N-dimethyl-*N*-N-*N*-trimethyl-6-O-glycolchitosan (GCPQ) [34] and probe sonication to yield a highly sensitive negative contrast agent. GCPQ consists of a glucosamine sugar backbone where, a fraction of the amine groups have been functionalised with either a long chained hydrophobic pendant group or a quaternary ammonium cation. Functionalisation in this way creates an amphiphilic polymer which self assembles into nanoparticles [35] and which enables drugs to cross biological barriers to produce formulations with a number of differentiating features [36–38]. The cationic polymer binds to the anionic surface of the precipitated SPIONs to form stable nano-sized clusters.

2. Experimental

2.1. Materials

All chemicals were obtained from Sigma Aldrich (UK), unless specifically stated and were used without further purification.

2.2. Methods

2.2.1. Synthesis of N-palmitoyl-N-monomethyl-N,N-dimethyl-N,N,N-trimethyl-6-O-glycolchitosan (GCPQ)

GCPQ was synthesised as described previously [34]. Briefly, glycol chitosan (5 g, M_w ~120 kDa, WAKO, Japan) was dissolved in 4 M HCl (380 mL). The solution was heated to 50 °C and stirred for 24 h. The resulting solution was dialysed exhaustively against water [molecular weight cut off (MWCO) = 3.5 kDa, 5 L, and 6 changes over 24 h] and then lyophilised to obtain degraded glycol chitosan (dGC) as a white fibrous solid. The molecular weight of dGC was measured using gel permeation chromatography with multi-angle laser light scattering (GPC-MALLS) as previously reported [34]. Yield = 46%, Mw = 7081 Da, Mw/ Mn = 1.011, dn/dc = 0.142 mL g^{-1}.

The degraded glycol chitosan (1 g) and $NaHCO_3$ (0.75 g) were dissolved in a mixture of ethanol and water (24 mL: 76 mL). Palmitic acid N-hydrosuccinimide (1.58 g, Toronto Research Chemicals, Canada) was dissolved in ethanol (300 mL) and was added drop wise to the glycol chitosan solution. The reaction was left to stir for 72 h protected from light. Ethanol was removed under vacuo and the aqueous phase extracted using diethyl ether (3 × 100 mL). The aqueous phase was dialysed exhaustively against water as described above and then lyophilised to obtain palmitoylated glycol chitosan (PGC) as a white fibrous solid. The palmitoylated glycol chitosan (300 mg) was dispersed in N-methyl-2-pyrrolidone (25 mL) and stirred vigorously overnight. Sodium hydroxide (40 mg) dissolved in ethanol (2 mL) and sodium iodide (45 mg) dissolved in ethanol (2 mL) were added to the solution and the mixture was heated to 36 ^{O}C. Methyl iodide (0.45 mL) was added and the reaction was stirred under a N_2 environment for 3 h. The product was precipitated using diethyl ether and left over night. The resulting precipitate was washed three times with diethyl ether (50 mL), dispersed in water (100 mL) and dialysed exhaustively against water, as described above. The dialysate was passed through an Amberlite IRA-96 column to remove iodide and then lyophilised to obtain GCPQ as a white fibrous solid. The molecular weight of GCPQ was measured using gel permeation chromatography with multi-angle laser light scattering (GPC-MALLS) as previously reported [34]. The synthesis had a total synthetic yield of 30%, Mw = 10,250, Mw/ Mn = 1.032, dn/dc = 0.156 mL g^{-1}.

2.2.2. Synthesis of clustered iron oxide nanoparticles

SPIONs (Fe_3O_4) were made via co-precipitation using ferrous and ferric chloride salts and NH_4OH as the base. Briefly, solutions of $FeCl_3.6H_2O$ (2 g, 7.4 mmoles) and $FeCl_2.4H_2O$ (0.734 g, 3.7 mmoles) [Fe^{3+}: Fe^{2+} = 2:1] were made using deoxygenated water (200 mL) and mixed in a round bottom flask under a N_2 atmosphere. NH_4OH (25% v/ v, 10 mL) was added rapidly, resulting in a dark black precipitate forming. The reaction was allowed to proceed for 30 min. whilst vigorously stirring. The black precipitate was isolated with a strong magnet and washed with de-oxygenated water until a neutral pH was obtained. De-oxygenated water was obtained by purging distilled H_2O with a stream of N_2 for several hours. The particles were stored wet under deoxygenated conditions. Clustering was achieved by simply adding a dispersion of the SPIONs (10 mg mL^{-1}, 1 mL) to a dispersion

of GCPQ (0.1–5 mg mL^{-1}, 4 mL) followed by mixing using probe sonication for 10 min (2 × 5 min., 7 µm amplitude, Soniprep 150, Fisher Scientific, UK.) to yield a black formulation.

2.2.3. Transmission electron microscopy

Images were collected using a FEI CM120 BioTwin Transmission Electron Microscope (Ex. Philips, The Netherlands). Digital images were captured using an AMT digital camera. A drop of the sample was placed on Formvar©/ Carbon Coated Grid (F196/100 3.05 mm, mesh 300, Tab Labs Ltd, UK). Samples were stained with 1% aqueous uranyl acetate, where indicated.

2.2.4. Dynamic light scattering

Particle size was determined by dynamic light scattering (DLS) on a Malvern Zetasizer 3000HS (Malvern Instruments, UK) using a laser wavelength of 633 nm. Samples were inverted several times and then left to equilibrate for 10 s before particle sizing was carried out. The accuracy of the instrument was assessed periodically using latex beads (polystyrene, mean size: 0.2 µm) in a 50 mM sodium chloride disperse phase.

2.2.5. Zeta potential measurements

Particle zeta potential was measured using a Malvern Zetasizer 3000HS (Malvern Instruments, UK). Nanoparticles were manually titrated to various pH values using 0.1 M HCl and 0.1 M NaOH. Measurements were carried out in gold plated disposable capillary cells (Malvern Instruments, UK). The accuracy of the instrument was assessed periodically using a polystyrene zeta standard (Malvern Instruments, UK).

2.2.6. Magnetic properties

Magnetization curves were determined in a Quantum Design hybrid Superconducting Quantum Interference Device-Vibrating Sample Magnetometer (SQUID-VSM) at 300 K, with applied fields up to 7 T. Samples were lyophilised to obtain a dry product. Weighed samples of the dry product were placed into plastic capsules and measurements carried out in a straw sample holder.

2.2.7. X-ray diffraction

X-ray diffraction patterns were collected on an X-ray diffractometer (PanAlytical, UK) using CoKα radiation (λ = 1.79 Å). Samples were prepared by pressing dried powders on a zero background silicon wafer and diffraction patterns were collected within 20–100 2θ (degrees) range.

2.2.8. In vitro relaxivity measurements

Relaxivity measurements for the clustered iron oxide nanoparticles were performed at the ICPMS (Campus de Cronenbourg, Strasbourg, France) on a contrast agent analyser (minispec mq 60, Bruker, Germany) at 1.5 T at 37 ^{O}C. T2 values were collected using a spin-echo sequence. T1 values were obtained using an inversion recovery sequence. The relaxivities were plotted against the iron concentration and the relaxivities per concentration were determined from the gradient of the slope. Iron concentration was measured using the 1,10-phenanthroline iron quantification assay [39].

3. Results and discussion

3.1. Formulation and nanoparticle morphology

SPIONs were prepared via a room temperature alkaline chemical precipitation method and to minimise oxidation of the resulting nanoparticles the reaction was carried out in oxygen free conditions by purging all aqueous reagents with N_2 gas for several hours before use. After the addition of NH_4OH a black precipitate was immediately formed which could be isolated with a strong magnet and washed with de-oxygenated water until a neutral pH was obtained (Fig. 1a). Transmission electron microscopy imaging confirmed the presence of spherical nanoparticles with an average diameter of 8.4 ± 2.1 nm (Fig. 2a and b). These SPIONs aggregated to form non-colloidal aggregates which sedimented in the disperse phase (Fig. 1a). The high interfacial energy between the iron surface and the aqueous disperse phase led to this uncontrolled aggregation [40]. On addition of GCPQ to the aqueous dispersion of the SPIONs and probe sonication, controlled clustering and a colloidal formulation was observed (Figs. 1b, 2 c–f). The method yielded clustered SPIONs which were observed to have improved colloidal properties compared to the nanoprecipitated SPIONs alone (Fig. 1a and b). Uranyl acetate stained electron microscopy images provided evidence that the polymer encapsulated a number of nanoparticles within irregular shaped, but colloidal clusters (Fig. 2c–d). Probe sonication disaggregated the original nanoprecipitated aggregates (Fig. 1a) enabling the amphiphilic GCPQ to stabilise the surface of a cluster of SPIONs.

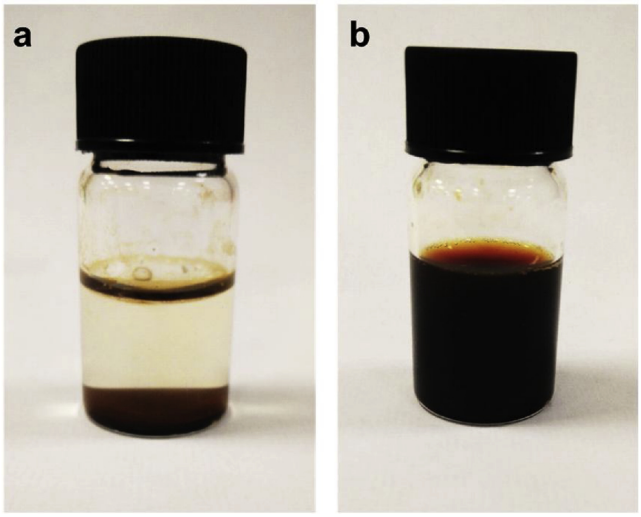

Fig. 1. (a) The nanoprecipitated SPIONs, (b) the clustered SPIONs after probe sonication with GCPQ (SPION, GCPQ ratio = 1: 0.04). The nanoprecipitated SPIONs form a sediment on the bottom of the vial, while the clustered SPIONs form a stable colloidal dispersion.

3.2. Nanoparticle size, stability and surface charge

Several aqueous clustered SPION formulations, containing different weight ratios of SPION, GCPQ (1: 2, 1: 0.4, 1: 0.2 and 1: 0.04) were formulated and sized via dynamic light scattering (DLS) over a 30-day period. Clustered SPION formulations made with polymer levels of less than a SPION, GCPQ ratio of 1: 0.04 were not stable and sedimented on Day 1 (data not shown). The various SPION formulations had initial sizes (and polydispersity indices in parenthesis) of 148 nm (0.19), 183 nm (0.22), 141 nm (0.19) and 152 nm (0.22), for SPION, GCPQ ratios of 1: 2, 1: 0.4, 1: 0.2 and 1: 0.04 respectively (Fig. 3a). The formulations remained colloidally stable and did not display any significant change in size over the time period ($p > 0.05$). This data suggests that a SPION, GCPQ ratio of at least 1:0.04 is needed to create a colloidally stable formulation and that higher levels of GCPQ did not lead to more stable clusters over the time period studied. These clustered SPIONs had a SPION content of up to 95% w/w (Fig. 3a); significantly higher than other clustered SPIONs reported. The latter of which contained a maximum SPION content of 54–57% w/w [16,41]. The surface charge of a nanoparticle is a driving factor of colloidal stability with a charged surface giving rise to colloidally stable dispersions due to charge repulsion [42]. The zeta potential or charge at the *slipping plane* is usually measured using electrophoresis. The slipping plane is a term used to describe the point at which counter ions strongly

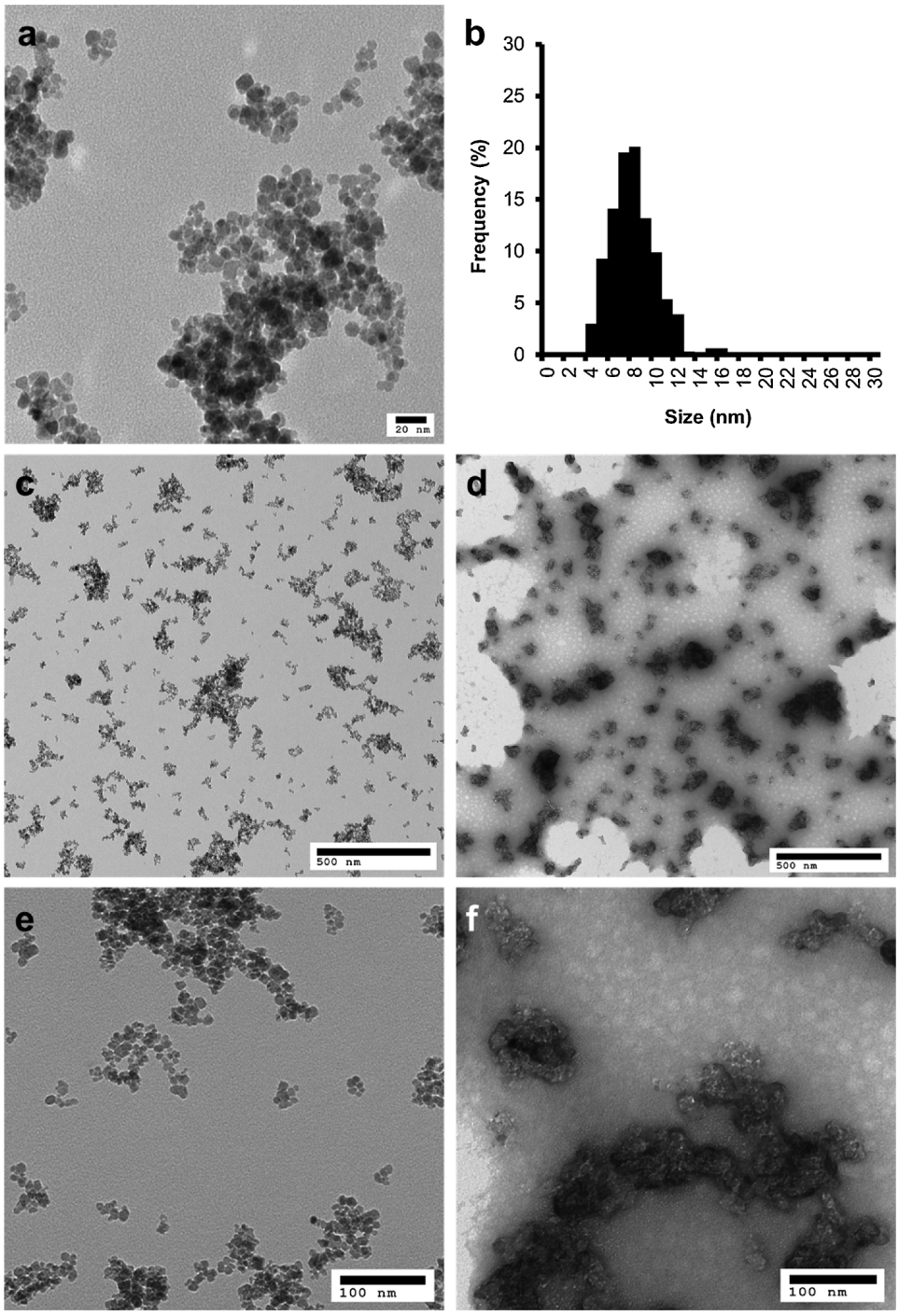

Fig. 2. (a) Transmission electron microscopy (TEM) image of the nanoprecipitated SPIONs - the high surface energy causes the nanoparticles to form large aggregates which settle on standing (Fig. 1a), (b) size distribution of the SPIONs with an average size of (8.4 ± 2.1) nm (mean ± s.d., n > 300), (c) TEM image of the clustered SPIONs (SPION, GCPQ ratio = 1: 0.04) - nano sized clustered SPIONs with various morphologies are observed, (d) TEM image of the clustered SPIONs (SPION, GCPQ ratio = 1: 0.04) stained with a 1% uranyl acetate, (e) TEM image of the clustered SPIONs (SPION, GCPQ ratio = 1: 0.04) at a higher magnification, (f) TEM image of the clustered SPIONs (SPION, GCPQ ratio = 1: 0.04) at a higher magnification stained with 1% uranyl acetate.

adsorbed to the nanoparticles' surface meet with loosely bound counter ions in the bulk phase [42]. The zeta potential is influenced profoundly by pH as surface molecules are ionised [43] and hence the pH should always be stated with zeta potential measurements. Distinctive sigmoidal curves are observed for both nanoparticle systems (Fig. 3b), with the clustered SPIONs displaying a strong positive zeta potential of (+22.5 ± 6.1 mV) at neutral pH (pH = 7.1) and the naked SPIONs have a weak negative (−4.3 ± 5.2 mV) zeta potential at neutral pH. The positive zeta potential is maintained even at alkaline pH, albeit weakening as the pH is increased and this is due to GCPQ's quaternary ammonium cationic functional group, as GCPQ has an apparent pKa of 5.99 ± 0.15 [34]. The zeta potential data provide further evidence of GCPQ clustering the SPIONs by coating them.

The current SPIONs, unusually have a hydrophilic coating prior to clustering with GCPQ and a weak negative surface charge (Fig. 3b) and hence GCPQ stabilises the cluster by an electrostatic attraction between the quaternary ammonium group on GCPQ and the negative charge on the surface of the nanoprecipitated SPIONs. Interactions between the hydroxyl groups of GCPQ and the hydroxyl groups on the surface of the SPIONs cannot be ruled out. While GCPQ stabilises the nanoprecipitated SPIONs from forming large aggregates, the controlled clustering of the SPIONs is facilitated by the hydrophobic interactions between the hydrophobic groups on GCPQ (N-palmitoyl). The hydrophobic parts of the cluster are shown by the areas devoid of stain on the negative stained image (Fig. 2f). While an amphiphilic polymer is utilised to effect clustering, it is clear from this work that a hydrophobically modified SPION surface is not essential for clustering as has been reported by others [16]. No additional separation steps were required for

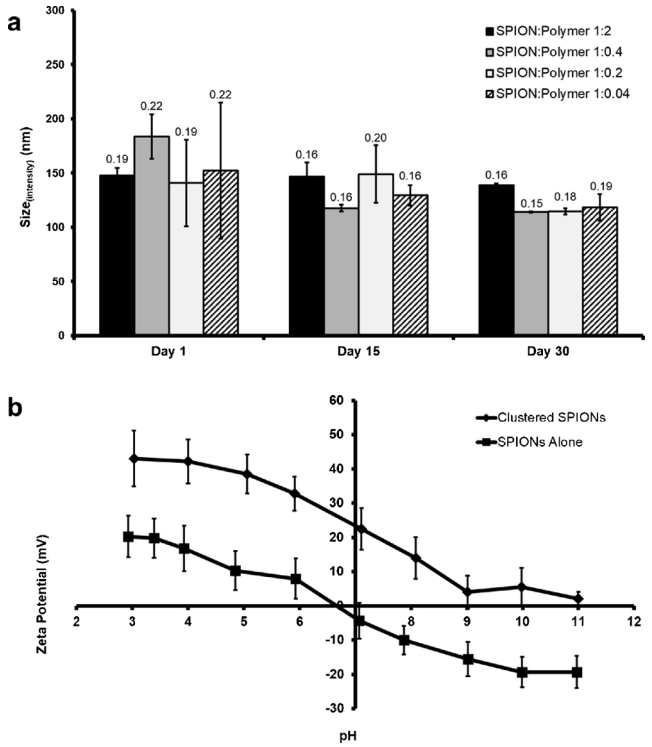

Fig. 3. (a) The mean size of clustered SPIONs at 5 ^{O}C with polydispersity values appearing above the bars. There were no significant differences observed in the size data over the time period (means ± s.d., n = 3, $p < 0.05$, 1-way ANOVA, Games-Howell post hoc test); (b) Zeta potential vs pH measurements (mean ± s.d., n = 3) on clustered SPIONs (SPION, GCPQ ratio = 1: 0.04). The clustered SPIONs have a positive zeta potential (+22.5 ± 6.1) mV at neutral pH (pH 7.1) and the nanoprecipitated SPIONs have a weakly negative charge (-4.3 ± 5.2) mV at neutral pH 7.1. Data are means ± s.d.

the SPIONs once prepared by nanoprecipitation and they were used as collected.

3.3. X-ray diffraction

We first decided to determine the crystal state of the clustered SPIONs in order to confirm the presence of magnetic iron oxide in the clusters. X-ray diffraction patterns were collected on the clustered and naked SPIONs and the presence of magnetic iron oxide (magnetite and/or maghemite) was confirmed in both samples (Fig. 4). The addition of polymer to the formulation has little effect on the crystallinity of the SPIONs. The average crystal size of the SPIONs calculated by the Scherrer equation was (8.8 ± 0.2) nm which is a very similar to the value obtained from TEM (8.4 ± 2.1) nm.

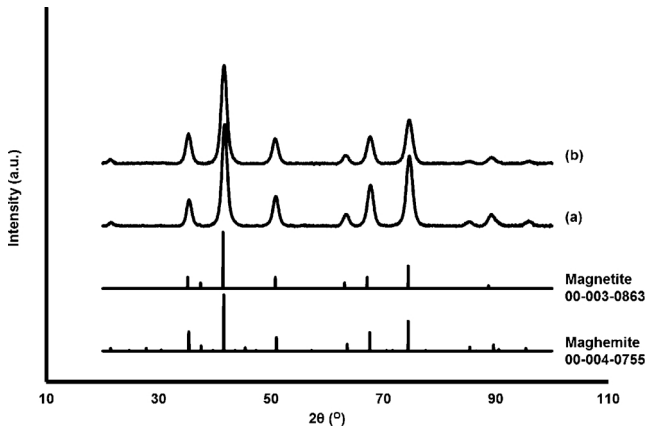

Fig. 4. X-ray diffraction patterns of (a) clustered SPIONs (SPION, GCPQ ratio = 1: 0.04) (b) nanoprecipitated SPIONs alone (8 nm). Both XRD patterns indicate the presence of magnetic iron oxide (magnetite or maghemite).

3.4. Magnetic characterisation

The magnetic behaviour of the clustered SPIONs was investigated by collecting field dependant magnetization plots (M vs H plots) using a super quantum interference device (SQUID). In its bulk phase magnetic iron oxide has *ferrimagnetic* properties, however when the size of an iron oxide particle is reduced to only a few nanometres (< 30 nm) it behaves rather differently and is said to be *superparamagnetic* [40]. Superparamagnetic materials become magnetised in the presence of an external magnetic field, however, unlike ferromagnetic and ferrimagnetic materials, superparamagnetic materials do not retain any magnetisation when the external magnetic field is removed. The overall bulk properties resemble that of paramagnetic materials. The key differences are that they are highly ordered at the molecular level and usually have much greater magnetic moments. Superparamagnetic materials are extremely desirable for biomedical applications as their magnetism can be manipulated "off/ on" in response to an external magnetic field. The clustered and naked SPIONs both displayed superparamagnetic behaviour with no observable remnant magnetisation, i.e. no hysteresis at 300 K (Fig. 5). The magnetic saturation of the SPIONs and the clustered SPIONs were found to be 73.3 ± 1.1 and 63.5 ± 1.3 emu g^{-1}, respectively. The small reduction in magnetisation is most likely due to the presence of GCPQ within the sample which will contribute to the overall mass but not the magnetisation of the material. These values are similar to those found for clustered SPIONs prepared using the traditional high temperature – organic solvent followed by micellization (63.7 emu g-^{1}) [16], encapsulation by phospholipids (73.7 emu g^{-1}) [21] or encapsulation in poly(L-lactide-co-glycolide) nanoparticles (˜40 emu g^{-1}) [19] or prepared by nanoprecipitation, heated to 110 °C and coated with 2,3-dimercaptosuccinic acid (65.4 emu g^{-1}) [22].

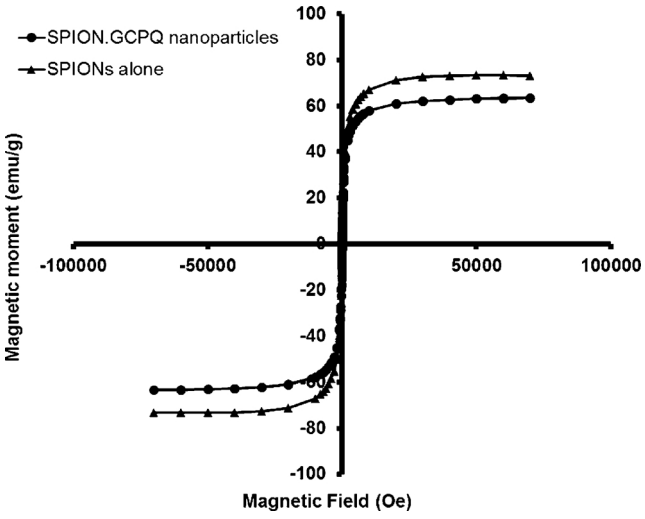

Fig. 5. M vs H plot at 300 K comparing the nanoprecipitated SPIONs alone to the clustered SPIONs. The nanoprecipitated SPIONs are superparamagnetic and retain their superparamagnetic behaviour after clustering with GCPQ. The magnetic saturation of the nanoprecipitated SPIONs and the clustered SPIONs was found to be 73.3 ± 1.1 emu g^{-1} and 63.5 ± 1.3 emu g^{-1}, respectively showing that the clustered SPIONs are less magnetic per gram of material. Data are means ± s.d., n = 3, ($p < 0.05$, Student's t-test).

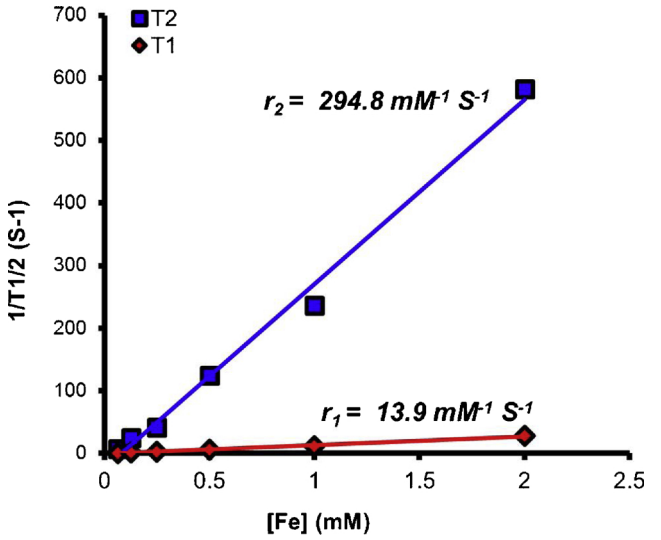

Fig. 6. Relaxivity plots of clustered SPIONs (SPION, GCPQ ratio = 1: 0.04) with relaxivities measured on a Bruker Mq 60 Minispectrometer (Bruker, Germany) at 37 °C. Plot of $1/T_1$ s^{-1} and $1/T_2$ s^{-1} against the concentration of a series of clustered SPIONs against [Fe]. The relaxivities (r_1 and r_2) can be determined from the slope of the plots.

3.5. In vitro relaxometry

MRI contrast agents act by altering the spin-lattice (longitudinal) relaxation time (T1) or longitudinal relaxation rates (relaxivities, 1/T1 = r_1) and spin-spin (transverse) relaxation time (T2) or transverse relaxation rates (relaxivities 1/T2 = r_2) of water protons in their vicinity [44]. A fundamental property of SPIONs is their ability to shorten the transverse relaxation time (T2) of water protons in their vicinity [7]. Clustered iron oxide nanoparticles show faster transverse (spin-spin) relaxivities (r_2) than single crystal iron oxide nanoparticles as the cluster behaves like a giant magnetised entity [45]. To investigate the MRI contrast ability of the clustered SPIONs, their r_1 and r_2 values were measured as a function of iron concentration using a contrast agent analyser (minispec mq 60, Bruker, Germany) at 1.5 T at 37 °C (Fig. 6). In vitro relaxivity measurements provide a powerful insight into the sensitivity and efficiency of a contrast agent in a controlled manner. The standard method for measuring relaxivity is by measuring the relaxation rates over a number of concentrations. The relationship between relaxation rates and concentration follows zero order kinetics and therefore, a plot of relaxation rates v concentration will give a straight line, where the relaxivity (r_1 or r_2) is the gradient. Overall, there was good correlation between concentration and relaxivity resulting in an r_1 value of 13.9 mM^{-1} s^{-1} and an r_2 value of 294.8 mM^{-1} s^{-1} hence, giving an r_2/r_1 of 21.1. MRI contrast agent materials with values of $r_2/r_1 < 10$ are generally considered to be applicable as positive contrast agents, while MRI contrast agent materials with $r_2/r_1 > 10$ are typically considered to be applicable as negative contrast agents [46]. The high r_2/r_1 value recorded here indicates that the clustered SPIONs would be effective T2 weighted contrast agents. The r_2 values compare favourably with the r_2 values of clustered SPIONs prepared using high temperature methods and measured on a 1.5 T instrument where values of 165 mM^{-1} s^{-1} were recorded for a 200 nm cluster of 8 nm SPIONs [41], 318 mM^{-1} s^{-1} for 100 nm clusters of 8 nm SPIONS [16], 294 mM^{-1} s^{-1} for 100 nm clusters of 7 nm particles [19] and 227 mM^{-1} s^{-1} for 50 nm clusters of 8 nm particles [47]. The r_2 values seen with the clustered SPIONs are significantly higher than those recorded for single SPION crystals (15.1 mM^{-1} S^{-1}) [18]. Clustering tends to reduce the longitudinal relaxivities [16,45] and this has been linked to the reduced access of water molecules to the SPIONs within the cluster [16]. The current clusters, however produced r_1 values that were larger than those recorded by others (13.9 mM^{-1} s^{-1}, Fig. 6) such as in the work of Ai et al [16] (1.3 – 3.0 mM^{-1} s^{-1} recorded at 1.5 T). We attribute this to the fact that the access of water molecules to SPIONs in the current clusters is not excessively hindered. When the r_2/r_1 ratios of commercially available T2 weighted contrast agents (r_2/r_1 = 1–9) [48] are considered, the current clustered SPIONs have superior r_2/r_1 ratios (r_2/r_1 = 21.1, Fig. 6) and so should be effective for MRI contrast applications.

This is the first report of clustered SPIONs prepared in aqueous media (in the absence of organic solvents) and at room temperature from nanoprecipitated SPIONs with high transverse relaxivity (r_2 > 200 mM^{-1} s^{-1}). Most of the previous reports of high r_2 relaxivity clusters involve the use of SPIONs prepared by thermal decomposition in high boiling point organic solvents at high temperatures (> 200 °C) followed by the use of aqueous based amphiphiles to extract the SPIONs and cluster the hydrophobically coated SPIONs within amphiphilic coatings [16,18]. The absence of organic solvents and the use of room temperature for the nanoprecipitation means that the current SPIONs will not have to involve further down-stream processing to remove residual organic solvents and do not require the high temperatures used in the thermal decomposition reactions. Alternative low temperature methods of producing clustered SPIONs, which similarly exclude organic solvents, also show relatively lower transverse relaxivities (r_2 < 200 mM^{-1} s^{-1}) [31–33].

4. Conclusions

SPIONs are useful for a number of biomedical applications and clustered SPIONs have been shown to be effective T2 weighted contrast agents with relaxivity ratios that are superior to single crystal materials. However, to achieve relatively high transverse relaxivities (r_2 > 200 mM^{-1} S^{-1}), the process of clustering requires organic solvents and high temperatures, limiting the industrial translation of clustered SPIONs. Here we report the facile room temperature and aqueous based preparation of clustered SPIONs and show that the resulting 150 nm clustered 8 nm SPIONs are superparamagnetic, have relaxivity ratios (r_2/r_1 = 21.1) that make them ideal for use as T2 weighted contrast agents and contain as much as 95% w/w iron oxide. We use nanoprecipitation and then probe sonication in the presence of an amphiphilic carbohydrate polymer, the chitosan amphiphile – GCPQ. The resulting clustered SPIONs are colloidally stable for at least 30 days.

Author contributions

N.J.H. was responsible for the design, synthesis, analysis and evaluation of the work reported in the study. X.W. was involved with experimental design and helpful discussions. I.F.U., A.G.S., N.T.K.T. & M.A. conceived and supervised the study. N.J.H. and I.F.U. wrote the manuscript.

Competing financial interests

The authors declare no competing financial interests

Acknowledgements

The Authors thank the EPSRC for a Ph.D. studentship under the Centre for Doctoral Training in Targeted Therapeutics & Formulation Sciences (EP/L01646X/1). This project was supported by AstraZeneca, UK. The authors would also like to thank David McCarthy for help with the TEM images and Paul Southern for his support with the SQUID.

References

[1] N.T.K. Thanh, Magnetic Nanoparticles: From Fabrication to Clinical Applications, Taylor & Francis, 2012.
[2] R.A. Revia, M. Zhang, Magnetite nanoparticles for cancer diagnosis, treatment, and treatment monitoring: recent advances, Mater. Today (Kidlington) 19 (2016) 157–168.
[3] B. Thiesen, A. Jordan, Clinical applications of magnetic nanoparticles for hyperthermia, Int. J. Hyperthermia 24 (2008) 467–474.
[4] M.H. Schwenk, Ferumoxytol: a new intravenous iron preparation for the treatment of iron deficiency anemia in patients with chronic kidney disease, Pharmacotherapy 30 (2010) 70–79.
[5] K. Ulbrich, K. Hola, V. Subr, A. Bakandritsos, J. Tucek, R. Zboril, Targeted drug delivery with polymers and magnetic nanoparticles: covalent and noncovalent approaches, release control, and clinical studies, Chem. Rev. 116 (2016) 5338–5431.
[6] S. Laurent, A.A. Saei, S. Behzadi, A. Panahifar, M. Mahmoudi, Superparamagnetic iron oxide nanoparticles for delivery of therapeutic agents: opportunities and challenges, Expert Opin. Drug Deliv. 11 (2014) 1449–1470.
[7] R. Jin, B. Lin, D. Li, H. Ai, Superparamagnetic iron oxide nanoparticles for MR imaging and therapy: design considerations and clinical applications, Curr. Opin. Pharmacol. 18 (2014) 18–27.
[8] F. Kiessling, M.E. Mertens, J. Grimm, T. Lammers, Nanoparticles for imaging: top or flop? Radiology 273 (2014) 10–28.
[9] Y.-X.J. Wang, Superparamagnetic iron oxide based MRI contrast agents: current status of clinical application, Quant. Imag. Med. Surg. 1 (2011) 35–40.
[10] Y.-X.J. Wang, Current status of superparamagnetic iron oxide contrast agents for liver magnetic resonance imaging, World J. Gastroenterol. 21 (2015) 13400–13402.
[11] Withdrawal Assessment Report for Sinerem Vol. 1 European Medicines Agency, 2008, pp. 1–18.
[12] R. Tietze, C. Alexiou, Improving cancer imaging with magnetic nanoparticles: where are we now? Nanomedicine (London) 12 (2017) 167–170.
[13] M. Rogosnitzky, S. Branch, Gadolinium-based contrast agent toxicity: a review of known and proposed mechanisms, Biometals 29 (2016) 365–376.
[14] N. Hobson, J. Weng, B. Siow, C. Veiga, M. Ashford, T.K. Nguyen, A.G. Schatzlein, I.F. Uchegbu, Clustering iron oxide nanoparticles leads to high contrast images, Nanomedicine (2019), https://doi.org/10.2217/nnm-2018-037.
[15] H. Wei, O.T. Bruns, M.G. Kaul, E.C. Hansen, M. Barch, A. Wisniowska, O. Chen, Y. Chen, N. Li, S. Okada, J.M. Cordero, M. Heine, C.T. Farrar, D.M. Montana, G. Adam, H. Ittrich, A. Jasanoff, P. Nielsen, M.G. Bawendi, Exceedingly small iron oxide nanoparticles as positive MRI contrast agents, Proc. Natl. Acad. Sci. U. S. A. 114 (2017) 2325–2330.
[16] H. Ai, C. Flask, B. Weinberg, X. Shuai, M.D. Pagel, D. Farrell, J. Duerk, J.M. Gao, Magnetite-loaded polymeric micelles as ultrasensitive magnetic-resonance probes, Adv. Mater. 17 (2005) 1949-+.
[17] S.H. Sun, H. Zeng, D.B. Robinson, S. Raoux, P.M. Rice, S.X. Wang, G.X. Li, Monodisperse MFe2O4 (M = Fe, Co, Mn) nanoparticles, J. Am. Chem. Soc. 126 (2004) 273–279.
[18] P.H. Qiu, C. Jensen, N. Charity, R. Towner, C.B. Mao, Oil phase evaporation-induced self-assembly of hydrophobic nanoparticles into spherical clusters with controlled surface chemistry in an oil-in-water dispersion and comparison of behaviors of individual and clustered Iron oxide nanoparticles, J. Am. Chem. Soc. 132 (2010) 17724–17732.
[19] R.R.T. Ragheb, D. Kim, A. Bandyopadhyay, H. Chahboune, B. Bulutoglu, H. Ezaldein, J.M. Criscione, T.M. Fahmy, Induced clustered nanoconfinement of superparamagnetic iron oxide in biodegradable nanoparticles enhances transverse relaxivity for targeted theranostics, Magn. Reson. Med. 70 (2013) 1748–1760.
[20] J.X. Fu, L. He, W.J. Xu, J.L. Zhuang, X.F. Yang, X.Z. Zhang, M.M. Wu, Y.D. Yin, Formation of colloidal nanocrystal clusters of iron oxide by controlled ligand stripping, Chem. Commun. 52 (2016) 128–131.
[21] M. Hodenius, T. Hieronymus, M. Zenke, C. Becker, L. Elling, J. Bornemann, J.E. Wong, W. Richtering, U. Himmelreich, M. De Cuyper, Magnetically triggered clustering of biotinylated iron oxide nanoparticles in the presence of streptavidinylated enzymes, Nanotechnology 23 (2012).
[22] F. Xiong, C.Y. Yan, J.L. Tian, K.K. Geng, Z.Y. Zhu, L.N. Song, Y. Zhang, M. Mulvale, N. Gu, 2, 3-Dimercaptosuccinic acid-modified Iron oxide clusters for magnetic resonance imaging, J. Pharm. Sci. 103 (2014) 4030–4037.
[23] F.C. Meldrum, B.R. Heywood, S. Mann, Magnetoferritin – invitro synthesis of a novel magnetic protein, Science 257 (1992) 522–523.
[24] S. Tahka, A. Laiho, M.A. Kostiainen, Diblock-copolymer-mediated self-assembly of protein-stabilized iron oxide nanoparticle clusters for magnetic resonance imaging, Chem. Eur. J. 20 (2014) 2718–2722.
[25] A.F. Palomec-Garfias, K.V. Jardim, M.H. Sousa, C. Márquez-Beltrán, Influence of polyelectrolyte chains on surface charge and magnetization of iron oxide nanostructures, Colloids Surf. A: Physicochem. Eng. Aspects 549 (2018) 13–24.
[26] J.R. Sosa-Acosta, J.A. Silva, L. Fernández-Izquierdo, S. Díaz-Castañón, M. Ortiz, J.C. Zuaznabar-Gardona, A.M. Díaz-García, Iron Oxide Nanoparticles (IONPs) with potential applications in plasmid DNA isolation, Colloids Surf. A: Physicochem. Eng. Aspects 545 (2018) 167–178.
[27] L.M. Sanchez, D.A. Martin, V.A. Alvarez, J.S. Gonzalez, Polyacrylic acid-coated iron oxide magnetic nanoparticles: the polymer molecular weight influence, Colloids Surf. A: Physicochem. Eng. Aspects 543 (2018) 28–37.
[28] W.E.M. Elsayed, F.S. Al-Hazmi, L.S. Memesh, L.M. Bronstein, A novel approach for rapid green synthesis of nearly mono-disperse iron oxide magnetic nanocubes with remarkable surface magnetic anisotropy density for enhancing hyperthermia performance, Colloids Surf. A: Physicochem. Eng. Aspects 529 (2017) 239–245.
[29] Y. Li, K. Hu, B. Chen, Y. Liang, F. Fan, J. Sun, Y. Zhang, N. Gu, Fe3O4@PSC nanoparticle clusters with enhanced magnetic properties prepared by alternating-current magnetic field assisted co-precipitation, Colloids Surf. A: Physicochem. Eng. Aspects 520 (2017) 348–354.
[30] E. Woźniak, M. Špírková, M. Šlouf, V.M. Garamus, M. Šafaříková, I. Šafařík, M. Štěpánek, Stabilization of aqueous dispersions of poly(methacrylic acid)-coated iron oxide nanoparticles by double hydrophilic block polyelectrolyte poly(ethylene oxide)-block-poly(N-methyl-2-vinylpyridinium iodide), Colloids Surf. A: Physicochem. Eng. Aspects 514 (2017) 32–37.
[31] D. Ni, W. Bu, E.B. Ehlerding, W. Cai, J. Shi, Engineering of inorganic nanoparticles as magnetic resonance imaging contrast agents, Chem. Soc. Rev. 46 (2017) 7438–7468.
[32] L. Li, W. Jiang, K. Luo, H. Song, F. Lan, Y. Wu, Z. Gu, Superparamagnetic iron oxide nanoparticles as MRI contrast agents for non-invasive stem cell labeling and tracking, Theranostics 3 (2013) 595–615.
[33] C. Corot, P. Robert, J.M. Idee, M. Port, Recent advances in iron oxide nanocrystal technology for medical imaging, Adv. Drug Deliv. Rev. 58 (2006) 1471–1504.
[34] K.W. Chooi, M.I. Simao Carlos, R. Soundararajan, S. Gaisford, N. Arifin, A.G. Schatzlein, I.F. Uchegbu, Physical characterisation and long-term stability studies on quaternary ammonium palmitoyl glycol chitosan (GCPQ)–a new drug delivery polymer, J. Pharm. Sci. 103 (2014) 2296–2306.
[35] X.Z. Qu, V.V. Khutoryanskiy, A. Stewart, S. Rahman, B. Papahadjopoulos-Sternberg, C. Dufes, D. McCarthy, C.G. Wilson, R. Lyons, K.C. Carter, A. Schatzlein, I.F. Uchegbu, Carbohydrate-based micelle clusters which enhance hydrophobic drug bioavailability by up to 1 order of magnitude, Biomacromolecules 7 (2006) 3452–3459.
[36] F.A. Fisusi, A. Siew, K.W. Chooi, O. Okubanjo, N. Garrett, K. Lalatsa, D. Serrano, I. Summers, J. Moger, P. Stapleton, R. Satchi-Fainaro, A.G. Schatzlein, I.F. Uchegbu, Lomustine nanoparticles enable both bone marrow sparing and high brain drug levels - a strategy for brain cancer treatments, Pharm. Res. 33 (2016) 1289–1303.
[37] D.R. Serrano, A. Lalatsa, M.A. Dea-Ayuela, P.E. Bilbao-Ramos, N.L. Garrett, J. Moger, J. Guarro, J. Capilla, M.P. Ballesteros, A.G. Schatzlein, F. Bolas, J.J. Torrado, I.F. Uchegbu, Oral particle uptake and organ targeting drives the activity of amphotericin B nanoparticles, J. Mol. Pharm. Org. Process Res. 12 (2015) 420–431.
[38] L. Godfrey, A. Iannitelli, N.L. Garrett, J. Moger, I. Imbert, T. King, F. Porreca, R. Soundararajan, A. Lalatsa, A.G. Schatzlein, I.F. Uchegbu, Nanoparticulate peptide delivery exclusively to the brain produces tolerance free analgesia, J. Control. Release 270 (2017) 135–144.
[39] D.H. Caldwell, R.B. Adams, Colorimetric determination of iron in water with o-phenanthroline, J. Am. Water Work. Assoc. 38 (1946) 727–730.
[40] A.K. Gupta, M. Gupta, Synthesis and surface engineering of iron oxide nanoparticles for biomedical applications, Biomaterials 26 (2005) 3995–4021.
[41] T.A. Meyer, C.A. Quinto, G. Bao, Control of Iron oxide nanoparticle clustering using dual solvent exchange, IEEE Magn. Lett. 7 (2016).
[42] A.T. Florence, D. Attwood, Physicochemical Principles of Pharmacy, 4th edition ed., McMillan Press, Ltd, London, 2006.
[43] C. Pfeiffer, C. Rehbock, D. Hühn, C. Carrillo-Carrion, D.J. de Aberasturi, V. Merk, S. Barcikowski, W.J. Parak, Interaction of colloidal nanoparticles with their local environment: the (ionic) nanoenvironment around nanoparticles is different from bulk and determines the physico-chemical properties of the nanoparticles, J. R. Soc. Interface 11 (2014).
[44] J.K. Lee, Recent advances in magnetic resonance imaging of renal masses, Can. Assoc. Radiol. J. 42 (1991) 185–189.
[45] A. Roch, Y. Gossuin, R.N. Muller, P. Gillis, Superparamagnetic colloid suspensions: water magnetic relaxation and clustering, J. Magn. Magn. Mater. 293 (2005) 532–539.
[46] U.I. Tromsdorf, O.T. Bruns, S.C. Salmen, U. Beisiegel, H. Weller, A. Highly Effective, Nontoxic T1 MR contrast agent based on ultrasmall PEGylated iron oxide nanoparticles, Nano Lett. 9 (2009) 4434–4440.
[47] D. Wang, B.B. Lin, T.P. Shen, J. Wu, F.H. Hao, C.C. Xia, Q.Y. Gong, H.R. Tang, B. Song, H. Ai, Control of the interparticle spacing in superparamagnetic iron oxide nanoparticle clusters by surface ligand engineering, Chin. Phys. B 25 (2016).
[48] M. Rohrer, H. Bauer, J. Mintorovitch, M. Requardt, H.J. Weinmann, Comparison of magnetic properties of MRI contrast media solutions at different magnetic field strengths, Invest. Radiol. 40 (2005) 715–724.